

# Multiplicity Functions and X-ray emission of Clusters, Groups and Galaxies

**P. Valageas and R. Schaeffer**

Service de Physique Théorique, CEN Saclay, 91191 Gif-sur-Yvette, France

Received / Accepted

**Abstract.** We use a new analytical formulation - discussed in previous papers- for the multiplicity functions of clusters and galaxies. This method is free from the cloud-in-cloud problem encountered in earlier approaches and well adapted to the description of the non-linear clustering features. It is especially suited to simultaneously describe rich clusters, groups and galaxies, consistently with the hierarchical picture of gravitational clustering and their evolution in time. Using a simple model for the X-ray luminosity (taking into account entropy considerations), we compare the temperature and luminosity distributions of rich clusters to observations. We find that, while rich clusters are cooling now, galaxy groups have cooled in the past where they were much more luminous and galaxies, that cool within a Hubble time at formation, also were X-ray emitters in the remote past. These features are potentially observable.

**Key words:** galaxies: clusters - galaxies: evolution - cosmology: large-scale structure of Universe - cosmic microwave background

## 1. Introduction

Clusters of galaxies are the largest virialized objects, characterized by scales which have just entered the non-linear regime. Thus, they are very rare and their number density is very sensitive to the cosmological parameters and to the amplitude of the initial density fluctuations (within the framework of the usual hierarchical scenarios). As a consequence, many authors have compared observations with predictions from numerical simulations (e.g. Eke et al.1996) or analytic approaches (e.g. Oukbir et al.1997) in order to obtain constraints on  $(\Omega_0, \Omega_\Lambda)$  and on the initial power-spectrum  $P(k)$ . However, the cluster temperature - X-ray luminosity relation involves non-gravitational effects since simple scaling laws (Kaiser 1986) recovered by numerical simulations (Eke et al.1998) which neglect radiative cooling and supernova or quasar feedback disagree with observations. This could be due to a preheating of the IGM by QSOs or supernovae (Valageas & Silk 1999b;

Cavaliere et al.1997; Ponman et al.1999) which is not considered yet by numerical simulations. Thus, analytic approaches are still needed in order to describe clusters. Moreover, they explicitly show the connection of cluster characteristics (e.g. their mass function) with other features of the universe (e.g. various properties of the underlying density field, of galaxies or quasars).

The standard way to estimate by analytical means the mass multiplicity function of collapsed objects is the well-known Press-Schechter (1974) approximation -hereafter PS- that directly recognizes the overdensities that will eventually collapse in the initial, linear, fluctuations of the density field. This approximation, however, suffers from many drawbacks. One is that it is customary -and necessary in order to bring the analytical form in agreement with numerical simulations- to multiply the result by an ad-hoc factor of two. This cannot be justified by the standard excursion sets argument for realistic filters like the top-hat in real-space as shown in Valageas & Schaeffer (1997) -hereafter VS- (see also Peacock & Heavens 1990). Indeed, in such a case the excursion sets imply a renormalization factor which goes to unity at large masses. Moreover, numerical results show some discrepancy with the PS predictions (Governato et al.1999).

Another fundamental problem, inherently related to hierarchical clustering, is to describe objects embedded within other, less dense but nevertheless virialized, objects, that is to describe *subclustering*. This has for long been known (Bardeen et al.1986) not to be reliable within approaches directly based on a recognition of the linear overdensities that will form objects, and is called the *cloud-in-cloud problem*. An approach based on counting overdensities in the linear regime leads to severe overcounting, so severe that the same objects are erroneously counted infinitely many times (VS). Thus, to describe an universe made of dense ( $10^4$  times the mean) galaxies as well as of galaxy clusters ( $10^2$  times the mean density) is out of reach of such approaches, while the description of intermediate objects such as Ly $\alpha$  clouds, that may have densities even below the mean, is unthinkable within this framework. Note indeed that the PS approximation can only deal with just-virialized halos.

Recent progress (VS) in the description of the non-linear density field, through a *non-linear scaling model* based on earlier approaches (Schaeffer 1984; Balian & Schaeffer 1989; Bernardeau & Schaeffer 1991), with an understanding of its relation to the initial spectrum of fluctuations, leads to analytical expressions that enable one to *directly count the overdensities in the actual non-linear density field*. The result exhibits many analogies with the PS approximation, but gives the correct result for the normalization and solves as well the cloud-in-cloud problem (there are no divergences). It also provides for the correlations of these objects and the associated bias as compared to the matter distribution (Bernardeau & Schaeffer 1992; 1999).

For the purposes of the present paper, the scaling approach gives a clear answer to the following problem. Choose a density contrast  $1 + \Delta = \rho/\bar{\rho}$  and define objects as having an inner density contrast larger than this threshold. Then *all* the mass in the universe (except a nonvanishing but negligible fraction in the very underdense regions) lies within such objects, that have a distribution of mass or size given by the theory. The choice of a larger contrast results in a different partition of the same mass into smaller objects, the procedure being valid for arbitrarily large contrasts (with obvious limits at the kpc scale since pressure and angular momentum are ignored). This is the way *subclustering* can be properly accounted for. The same theory can then simultaneously describe virialized clusters, which have a contrast of  $\simeq 200$ , as well as galaxies (Valageas & Schaeffer 1999), whose contrast is  $\simeq 5000$ , embedded or not in the latter objects. The procedure holds also for small density contrasts, even negative, provided one is at scales (in the present universe, for instance, not much above 1 Mpc) where the correlation function is large enough so as to insure one is in the fully non-linear regime. The new feature introduced by the scaling model is that, because one directly works in the non-linear regime, this separation can be done properly. The same procedure applied to future non-linear objects in the linear regime as is done in the PS approach would lead to the above mentioned divergences (VS), which is another indication that defining objects directly in the linear regime as is done in the latter approach is unsecure. The proper description of the non-linear density field shows for instance that within large condensations there is extremely strong subclustering. It also predicts *underdense non-linear objects* embedded in much less dense, nearly void regions.

The analytical predictions of the scaling model have been checked against numerical simulations (Valageas, Lacey & Schaeffer 1999) under the most extreme conditions, searching for non-linear objects with density contrasts ranging from values as large as  $1 + \Delta = 5000$  down to  $1 + \Delta = 0.5$ , spanning four orders of magnitude, limited only by the accuracy of the simulation. They are indeed seen to provide reasonable results, at least in the

above range, allowing to describe non linear objects and their evolution. These theoretical predictions are also in the line of the findings of Moore et al.(1998) that resolve some of the structure of dark matter halos in their simulation. As a consequence, the mass functions provided by this approach give, with the same parameters, a unified description of vastly different objects, such as galaxies and quasars (Valageas & Schaeffer 1999), Ly $\alpha$  clouds (Valageas, Schaeffer & Silk 1999), the ionization flux emitted by QSO's (Valageas & Silk 1999a), allowing for a consistent picture of the reheating and the reionization history of the universe (Valageas & Silk 1999a,b). Although this had been checked from the beginning of this series of articles, it remains to be explicitly shown that the same approach, without new parameters, provides for the correct cluster multiplicity and for its observed evolution.

Thus, the main goals of this article are to:

- investigate an analytic method which can describe in a consistent way the mass functions of clusters, galaxies..., while making the connection with other properties of the density field (correlation functions, counts-in-cells,...).
- introduce a simple model which can reproduce the observed temperature - X-ray luminosity relation of groups and clusters.
- use the global scope of our description to compare the X-ray emission provided by clusters, groups, galaxies and quasars.

In Sect.2, we present the expressions of the multiplicity functions, comparing the PS approach and the scaling model. Sect.3 is devoted to a short description of our modelling of rich clusters and galaxy groups. The X-ray temperature function is presented in Sect.4, together with its evolution. A detailed comparison is made between the PS and the scaling model predictions. In Sect.5, we give the predictions for the mass function evolution. Sect.6 presents the X-ray emission while Sect.7 is devoted to the implications of our model for the characteristics of the Sunyaev-Zel'dovich effect. We also estimate the counts along the line-of-sight in Sect.8. Finally, since our model predicts the X-ray emission at early times due to quasars and *cooling galaxies*, the intensity of the latter contribution is compared with the one that originates from clusters and groups in Sect.9.

## 2. Multiplicity functions

We shall define clusters as halos with a mean density contrast equal to  $\Delta_c$ , where  $\Delta_c$  is the density contrast at the time of virialization, at the redshift  $z$  we consider, given by the spherical collapse model. This means that clusters just virialize at the redshift at which we see them and some material may still be falling onto the overdensity at its boundary. For a critical universe this density threshold is a constant:  $\Delta_c \simeq 177$ . Numerical simulations show that this value of the density contrast separates reasonably well the virialized halos from the surrounding mate-

rial still falling onto the overdensity (Cole & Lacey 1996). This justifies this traditional definition of clusters.

Following the method outlined in VS we shall use two prescriptions to get the comoving mass function of these halos. First, the usual PS approximation gives:

$$\eta(M) \frac{dM}{M} = \sqrt{\frac{2}{\pi}} \frac{\bar{\rho}_0}{M} \frac{\delta_c}{\sigma} \left| \frac{d \ln \sigma}{d \ln M} \right| \exp \left[ -\frac{\delta_c^2}{2\sigma^2} \right] \frac{dM}{M} \quad (1)$$

where  $\delta_c(z)$  is the present linear density contrast for halos which collapse at redshift  $z$ , according to the spherical collapse model, and  $\bar{\rho}_0$  is the mean density of the universe at  $z = 0$ . As usual,  $\sigma(M)$  is the rms density fluctuation extrapolated by linear theory at  $z = 0$  at scale  $M$ . Here we multiplied the mass function (1) by the usual empirical factor of 2 so that all the mass is contained in such overdensities.

The second prescription we use, which we shall call the *scaling model*, assumes that the many-body correlation functions follow specific scaling laws obtained from the stable-clustering ansatz (see VS for details). Then, we attach to each object a parameter  $x$  defined by:

$$x(M, z) = \frac{1 + \Delta_c}{\bar{\xi}[R(M, z), z]} \quad (2)$$

where

$$\bar{\xi}(R) = \int_V \frac{d^3 r_1 d^3 r_2}{V^2} \xi_2(\mathbf{r}_1, \mathbf{r}_2) \quad \text{with} \quad V = \frac{4}{3} \pi R^3$$

is the average of the two-body correlation function  $\xi_2(\mathbf{r}_1, \mathbf{r}_2)$  over a spherical cell of radius  $R$  and provides the measure of the density fluctuations in such a cell. Then, we write the multiplicity function of these objects (which are defined by the density threshold  $\Delta_c$ ) as (see VS):

$$\eta(M) \frac{dM}{M} = \frac{\bar{\rho}_0}{M} x^2 H(x) \frac{dx}{x} \quad (3)$$

The scaling function  $H(x)$  only depends on the initial spectrum of the density fluctuations and must be obtained from numerical simulations. However, from theoretical arguments (see VS, Bernardeau & Schaeffer 1992 and Balian & Schaeffer 1989) it is expected to follow the asymptotic behaviour:

$$x \ll 1 : H(x) \propto x^{\omega-2} \quad , \quad x \gg 1 : H(x) \propto x^{\omega_s-1} e^{-x/x_*}$$

with  $\omega \simeq 0.5$ ,  $\omega_s \sim -3/2$ ,  $x_* \sim 10$  to 20 and by definition it must satisfy

$$\int_0^\infty x H(x) dx = 1 \quad (4)$$

This formulation is directly linked to the statistics of the counts-in-cells which involve a scaling function  $h(x)$ , related to the probability  $P(\Delta, R)$  to have a density contrast  $1 + \Delta$  in a spherical cell of fixed radius  $R$ , that scales as

$$(1 + \Delta) P(\Delta, R) d\Delta = x^2 h(x) \frac{dx}{x} \quad , \quad x(\Delta) = \frac{1 + \Delta}{\bar{\xi}[R, z]} \quad (5)$$

This function  $h(x)$  is very close to  $H(x)$ , see VS and Valageas et al.(1999a) for details. It has been checked against numerical simulations for CDM initial conditions by Bouchet et al.(1991) and, more systematically using power-law initial spectra in Colombi et al.(1997), Munshi et al.(1999) and Valageas et al.(1999a). Here we note that this prescription applies to the highly non-linear regime ( $\bar{\xi} > 100$ ) while clusters correspond to mildly non-linear scales (e.g.  $\bar{\xi} \sim 10 - 100$ ). Hence the mass functions we obtain may show an accuracy of 10%. Note however that the scaling function we shall use, taken from numerical simulations by Bouchet et al.(1991), was measured in this range of  $\bar{\xi}$ .

### 3. Characteristics of the halos

We assume that the dark matter halos have a mean isothermal density profile  $\rho(r) \propto r^{-2}$ . Then we write for the velocity dispersion of the dark matter:

$$\frac{d}{dr}(\rho \sigma_v^2) = -\rho \frac{GM(< r)}{r^2} \quad (6)$$

which leads to

$$\sigma_v^2(R) = \frac{GM}{2R} \quad (7)$$

We also define the virial temperature  $T$  of the halo by  $kT = \mu m_p \sigma_v^2$ , where  $\mu m_p$  is the mean molecular weight of the gas and  $m_p$  the proton mass:

$$kT = \frac{\mathcal{G} \mu m_p M}{2R} \quad (8)$$

We assume that the mass of baryons  $M_b$  is proportional to the mass of the dark matter halo  $M$ :

$$M_b = \frac{\Omega_b}{\Omega_0} M \quad (9)$$

where  $\Omega_b$  is the present ratio of the baryon density to the critical density. With these parameters, using the fact that halos are defined by the density contrast  $\Delta_c(z)$ , we have:

$$M \propto \Omega_0 (1 + \Delta_c)(1 + z)^3 R^3 \quad (10)$$

where  $R$  is the virial radius of the cluster, and eq.(8) writes:

$$T = T_s M_{15}^{2/3} \Delta_c(z)^{1/3} (1 + z) \quad (11)$$

with

$$M_{15} = \left( \frac{M}{10^{15} M_\odot} \right) \quad \text{and} \quad T_s = 1.2 \Omega_0^{1/3} h^{2/3} \text{ keV}$$

This is consistent with numerical simulations which recover this scaling law, with a similar normalization. In these units, Navarro et al.(1995) find  $T_s = 1.4 \Omega_0^{1/3} h^{2/3}$  keV while Evrard et al.(1996) get  $T_s = 1.2 \Omega_0^{1/3} h^{2/3}$  keV.

We shall use two cosmologies. First we study a critical universe with  $\Omega_b = 0.04$ ,  $H_0 = 60$  km/s,  $\sigma_8 = 0.5$  and a

CDM power-spectrum (Davis et al.1985). Next we use an open CDM universe with  $\Omega_0 = 0.3$ ,  $\Omega_\Lambda = 0$ ,  $\Omega_b = 0.03$ ,  $H_0 = 60$  km/s and  $\sigma_8 = 0.77$ . These values are those we used in previous articles where we considered the luminosity functions of galaxies (Valageas & Schaeffer 1999), Lyman- $\alpha$  absorbers (Valageas et al.1999b) and reionization by stars and quasars (Valageas & Silk 1999a). Thus, this present study of clusters and groups of galaxies completes our description of structure formation in the universe, so that we obtain a unified model which can describe in a consistent fashion all these objects, from small low-density Lyman- $\alpha$  absorbers up to massive clusters.

#### 4. Evolution of the X-ray temperature function

Using  $\eta(T)dT/T = \eta(M)dM/M$  we can get the cluster temperature function from (11) and (1) or (3). Its evolution with redshift is shown in Fig.1 and Fig.2 for a CDM power-spectrum for both a critical and an open universe. Note that the temperature  $T$  we consider in this section is the virial temperature. Indeed, for the hot clusters ( $T \gtrsim 1$  keV) we study here it is also the temperature of the gas which is heated by shocks during the gravitational collapse. In contrast, in cool groups ( $T < 1$  keV) the gas is also influenced by a possible preheating of the IGM (e.g. Valageas & Silk 1999b) which leads to a smoother baryonic density profile and a larger gas temperature. This is discussed in Sect.6.

We can see that the *scaling mass function* (3) predicts more numerous very massive halos but fewer small objects than the PS mass function (1). This difference can be directly seen through the scaling function  $H(x)$ . Indeed, as shown in VS the PS formulation can be translated into the scaling approach in the highly non-linear regime where it leads to a specific scaling function:

$$h_{PS}(x) = \sqrt{\frac{2}{\pi}} \frac{5+n}{6\alpha} x^{\frac{5+n}{6}-2} \exp\left[-x^{(5+n)/3}/(2\alpha^2)\right] \quad (12)$$

where  $n$  is the slope of the power-spectrum and  $\alpha \simeq 1$ . A comparison with the function  $h(x)$  directly measured in numerical simulations from counts-in-cells (see VS and Valageas et al.1999a) shows that the large-mass cutoff of the PS mass function is too sharp while its peak (at masses  $M_*$  where  $\sigma(M_*) = 1$ ) is too high. This latter region corresponds to low mass clusters in Fig.1 and Fig.2. Note that at very low masses, corresponding to small galaxies, the PS mass functions gives more objects than the scaling prescription as seen in Valageas & Schaeffer (1999). We note that using numerical N-body simulations to study cluster mass functions Governato et al.(1999) found that for a standard CDM model ( $\Omega = 1$ ) normalized to  $\sigma_8 = 0.5$  (which is our case) the PS prescription underestimates the number of hot clusters  $kT > 7$  keV by almost a factor 10 at  $z = 1$ , while it overestimates the number of small halos. We can see in Fig.1 that we recover this trend. However, the discrepancy between our two mass functions is

slightly larger than what these numerical results imply at the large mass end. This may be due to the fact that the power-spectrum we use (from Davis et al.1985) is slightly different from theirs and to the use of our scaling model in a range of  $\bar{\xi}$  slightly beyond its range of validity: indeed very high masses correspond to large scales which are getting close to the linear regime where the scaling model is not valid. Nevertheless, the agreement of our predictions (already described in a more general context in VS) with the behaviour observed in the numerical simulations is quite encouraging. Governato et al.(1999) also found that the deficiency of massive halos predicted by the PS approach gets more severe for smaller  $\sigma_8$  (hence also at higher redshifts). In our view, this is simply due to the fact that in this case one looks at rarer objects, farther in the cutoff of the mass function, which increases the discrepancy between both mass functions which have different exponential tails.

We also note that one would naturally expect on general grounds some deviations from the PS prescription to occur. First, we recall that the multiplicative factor 2 introduced in the usual PS mass function is not justified by the excursion set results (Bond et al.1991) for a window function which is a top-hat in real space. Indeed, as shown in VS and noticed from numerical results by Peacock & Heavens (1990) the normalization problem vanishes for rare massive objects so that one should keep the PS mass function without the factor 2 in the high mass exponential tail. On the other hand, the “cloud-in-cloud” problem is very severe for small objects which means that the slope of the PS mass function in this regime has no significance (VS). Then, the PS formulation mainly states that i) regions of space which are within non-linear objects in the actual universe (defined by a density contrast  $|\Delta_c| \sim 1$  for instance) correspond to regions which have already turned non-linear according to the linear theory (they have a linear density contrast  $|\delta_c| \sim 1$ ) and ii) overdensities come from regions which were initially overdense. Both of these assumptions look very reasonable for just-collapsed objects, but are obviously insufficient to describe actual condensations since the subsequent non-linear evolution is totally ignored. The latter, clearly, will tend to yield more objects in the mass range where there are nearly none: the very large as well as the very small masses. The comparison of the PS and the scaling model approaches indeed shows that the multiplicity distribution is strongly modified for these masses. Note also that if the actual mass function predicts more numerous rare massive halos than the usual PS prescription it must lead to fewer objects in some range at smaller masses since both of them have the same normalization (they count a fraction unity of the mass of the universe). As noticed above, in our case the scaling mass function indeed predicts fewer intermediate halos (which appear as small objects in the figures) but at the very low mass end it leads to more numerous halos, see also VS. We recall here that the scaling func-

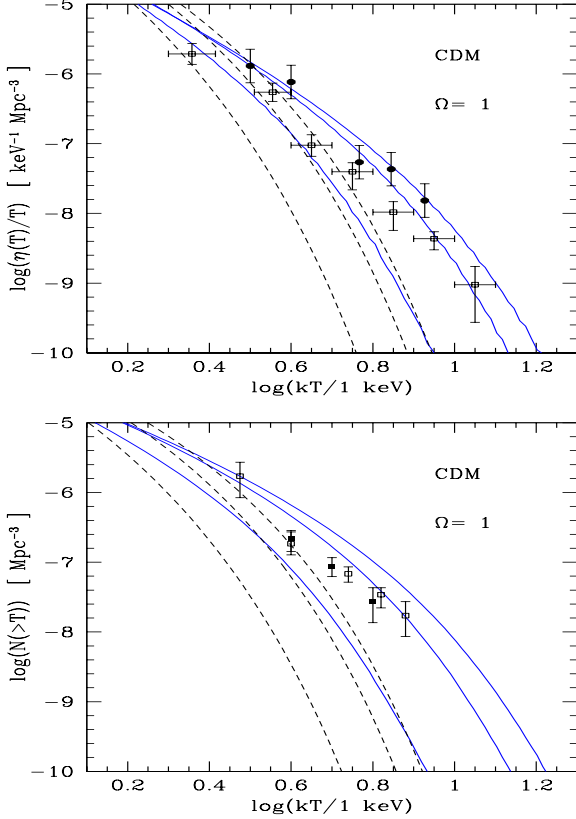


**Fig. 1.** *Upper panel:* the comoving cluster X-ray temperature function  $\eta(T) dT/T$  for a CDM power-spectrum in the case  $\Omega = 1$ . The solid lines correspond to the scaling prescription while the dashed lines represent the PS formulation. We display the redshifts  $z = 0.05$ ,  $z = 0.33$  and  $z = 1$  (a larger  $z$  corresponds to fewer bright clusters). The data points are observational results at  $z = 0$  from Henry & Arnaud (1991) (disks) and Edge et al.(1990) (squares). *Lower panel:* the cumulative cluster temperature function at the same redshifts. The open and filled squares are observations from Henry (1997) at  $z = 0.05$  and  $z = 0.33$  respectively.

tion  $H(x)$  is obtained from numerical simulations and it relies on the assumption that the many-body correlation functions verify specific scaling laws (checked in these simulations). Thus there is no known method (yet) to derive  $H(x)$  analytically. However, the function  $H(x)$  we use is consistent with numerical results (in the range where it has been tested) by construction. The main advantages of this scaling approach are i) to make the link between the mass functions and the counts-in-cells statistics and ii) to provide a very powerfull tool which can describe many different mass functions (i.e. defined by various density thresholds) as well as other properties of the non-linear density field, see VS and Valageas et al.(1999a).

We can see in the figures that the redshift evolution is very sensitive on the cosmological parameter  $\Omega_0$ , as was

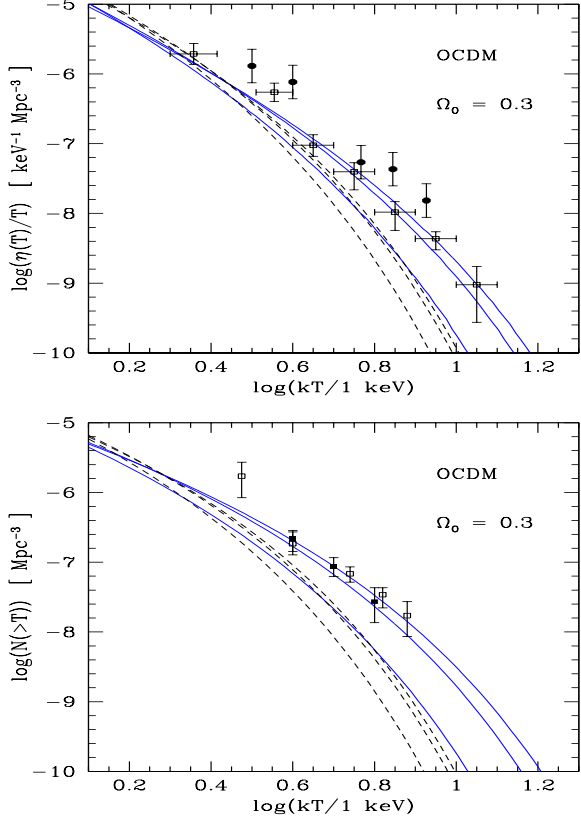


**Fig. 2.** The comoving differential and cumulative temperature functions as in Fig.1, for the case of an open universe with  $\Omega_0 = 0.3$ .

noticed by Eke et al.(1996) for instance. The number of clusters declines faster with  $z$  for the critical universe than for the open model. This is simply due to the fact that in the latter case structures have nearly stopped growing since the redshift where  $\Omega$  became appreciably smaller than unity, whence a very weak evolution with redshift, while in the former case structures keep building under the action of gravity at all epochs. Thus, the very small decline with  $z$  of the observed cluster temperature function (Henry 1997) from  $z = 0.05$  to  $z = 0.33$  favors the open case (or more generally a low-density universe). However, the redshift evolution of the cluster temperature function we obtain in the critical case is not much faster than the observed decline and our study shows it cannot be ruled out (taking into account the scatter in the data as well as the theoretical approximations involved). Note that we could obtain a better agreement with the data for  $\Omega = 1$  by choosing a slightly lower  $\sigma_8$ . However, the normalization of the power-spectrum we use is constrained by our previous studies of galaxies, quasars and Lyman- $\alpha$  clouds since we want to build a unified consistent model. Hence we must choose a value which provides good results for all these objects. Moreover, as explained in Sect.2 massive clusters correspond to midly non-linear scales close to the

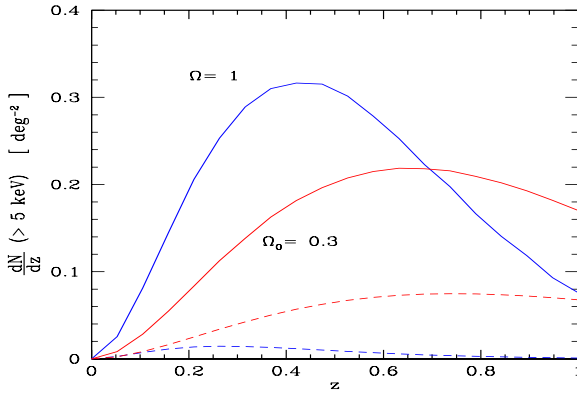


**Fig. 3.** The redshift distribution per square degree of clusters hotter than 5 keV, for  $\Omega = 1$  and  $\Omega_0 = 0.3$ ,  $\Omega_\Lambda = 0$ , with a CDM power-spectrum. The graph shows the number of clusters  $dN/dz(> 5 \text{ keV})$  per unit redshift interval and square degree. The solid lines correspond to the non-linear prescription while the dashed lines represent the PS formulation. The open universe corresponds to the slowest redshift evolution.

theoretical limit of validity of the scaling model, so that we may slightly overestimate the number of very massive clusters. Thus the value  $\sigma_8 = 0.5$  used for  $\Omega = 1$  (which is also the result obtained by the numerical simulation from Governato et al. 1999) seems satisfactory.

The dependence on  $\Omega_0$  of the redshift evolution of the cluster temperature function is even more apparent in Fig.3 which shows the redshift distribution of clusters hotter than 5 keV, per square degree, for both critical and open universes:

$$\frac{dN}{dz}(> 5 \text{ keV}) = \left( \frac{\pi}{180} \right)^2 \frac{dV}{d\Omega dz} \int_{5 \text{ keV}}^{\infty} \eta(T, z) \frac{dT}{T} \quad (13)$$

where  $dV/d\Omega dz$  is the comoving volume element per unit steradian and unit redshift. The normalization of the PS prediction is lower than for the scaling approach as explained above. The important result of this figure is to emphasize the difference of the redshift evolution between both cosmologies. Thus, for  $\Omega = 1$  the number of such clusters reaches a maximum at  $z = 0.4$  while for  $\Omega_0 = 0.3$  the peak corresponds to  $z = 0.65$  and the evolution is slower.

## 5. Evolution of the mass function

The redshift evolution of the comoving cluster mass function is shown in Fig.4. Of course, as was the case for the temperature functions the evolution is faster for the critical universe than for the open case. The redshift evolution of the mass function is faster than the change in the temperature function which was presented in Fig.1 and Fig.2. This is due to the temperature-mass relation (11) which gives  $T \propto M^{2/3} \Delta_c(z)^{1/3} (1+z)$ . Thus, the temperature

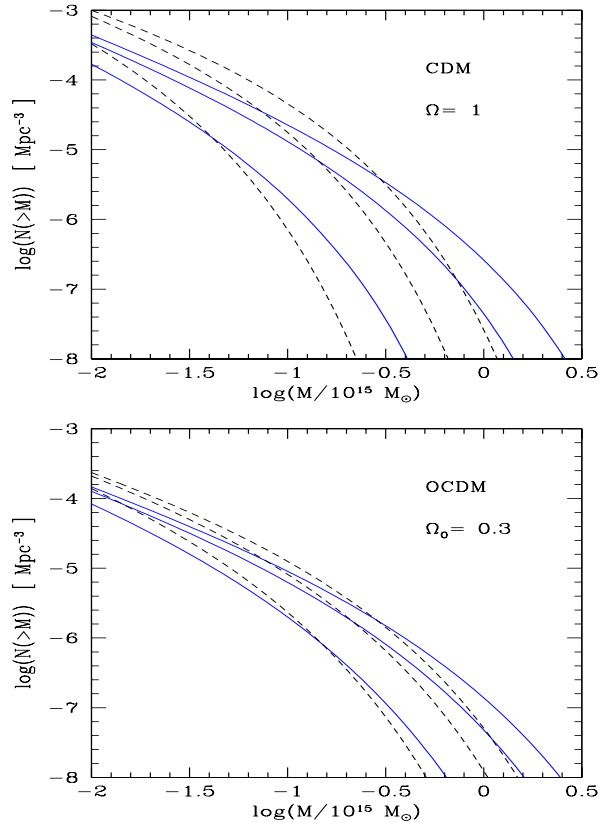


**Fig. 4.** *Upper panel:* the cluster comoving cumulative mass function at redshifts  $z = 0.05$ ,  $z = 0.33$  and  $z = 1$ , for a critical universe with a CDM power-spectrum. Higher redshifts lead to fewer massive clusters. The solid lines correspond to the scaling prescription while the dashed lines represent the PS formulation. *Lower panel:* same curves for an open universe with  $\Omega_0 = 0.3$ .

which corresponds to a given mass increases with  $z$ , which enhances the redshift evolution of the mass function. The scaling approach again predicts fewer low mass halos and more very massive objects than the PS prescription. In a similar fashion, Governato et al. (1999) find that the PS mass function overestimates the number of small clusters ( $M < 2 \cdot 10^{14} M_\odot$ , for  $\sigma_8 = 0.7$ ) and underestimates the number of massive halos (though the discrepancy they measure is smaller than ours). Of course, this behaviour is the direct consequence of the trend described in Sect.4 for the temperature multiplicity function.

The redshift distribution of clusters more massive than  $5 \cdot 10^{14} M_\odot$  is shown in Fig.5. Of course, as was the case in Fig.3 the evolution is slower for the low-density universe.

## 6. Evolution of the X-ray luminosity function

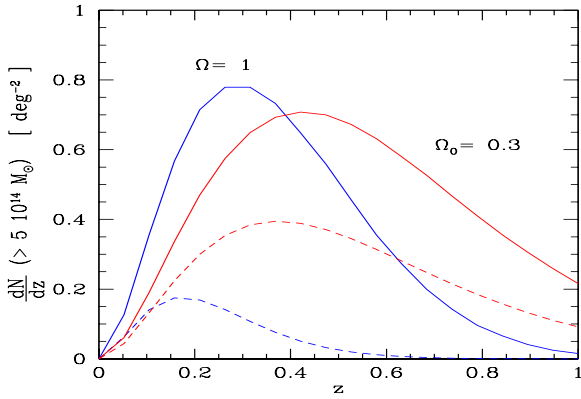


**Fig. 5.** The redshift distribution per square degree of clusters more massive than  $5 \times 10^{14} M_{\odot}$ , for  $\Omega = 1$  and  $\Omega_0 = 0.3$ . The graph shows the number of clusters  $dN/dz(> 5 \times 10^{14} M_{\odot})$  per unit redshift interval and square degree. The solid lines correspond to the non-linear precription, while the dashed lines represent the PS formulation. The open universe corresponds to the slowest redshift evolution.

### 6.1. The temperature-luminosity relation

The bolometric X-ray luminosity  $L_{bol}$  of a cluster of volume  $V$  is:

$$L_{bol} = \int_V n_e^2 \Lambda_b(T) dV \quad (14)$$

where  $n_e$  is the electron number density and  $\Lambda_b(T)$  is the bremsstrahlung emissivity function (in  $\text{erg cm}^3 \text{ s}^{-1}$ ). Thus, contrary to the Sunyaev-Zel'dovich effect, see (27), the X-ray luminosity strongly depends on the density profile of the hot gas within the cluster. Using (11) and the fact that  $\Lambda_b(T) \propto \sqrt{T}$  one expects (Kaiser 1986):

$$L_{bol} \propto T^2 \quad (15)$$

However, observations show a much steeper slope  $L_{bol} \propto T^{2.88}$  (Arnaud & Evrard 1999). Thus some physics is missing in the derivation leading to (15). It has been suggested in the litterature (e.g. Evrard & Henry 1991; Cavaliere et al. 1997; Ponman et al. 1999) that one needs to take into account the reheating of the IGM, prior to cluster formation, which raises its entropy and can modify the gas dynamics in cool clusters. Indeed, if this entropy “floor” is sufficiently large the gas is heated by the adiabatic compression up to a temperature which can be as large as the virial temperature of the halo. In this case the density profile of the gas is much smoother than the distribution of the dark matter, which diminishes the luminosity of these cool clusters and modifies the relation  $T - L_{bol}$ . Such a reheating of the IGM by quasars or supernovae was studied in Valageas & Silk (1999b) where it was shown that the energy provided by quasars may be sufficient to reheat the IGM. The energy delivered by supernovae was found by

the latter authors to be rather small, but a more thorough estimate is currently being done. An initially hot IGM or the intra-cluster supernovae act to reheat the cluster gas, and are relatively much more efficient for the smaller clusters where shocks can only heat the gas up to the virial temperature  $T$  of the halo during gravitational collapse. In order to take into account both of these effects, we simply write for the final temperature of the gas:

$$T_g(r) = T(r) + T_{ad} \quad (16)$$

where  $T_{ad} = 0.35 \text{ keV}$  and  $T(r)$  is the virial temperature due to the gravitational potential well. In order to obtain the density profile of the gas within the dark matter potential well we assume isothermal and hydrostatic equilibrium at the temperature  $T_g$  within a singular isothermal sphere for the dark matter halo (hence  $T(r)$  is constant and  $\rho \propto r^{-2}$ ). Thus we write:

$$\frac{dP}{dr} = -\rho_g \frac{\mathcal{G}M(< r)}{r^2} \quad \text{with} \quad P = \frac{\rho_g k T_g}{\mu m_p} \quad (17)$$

where  $P$  is the pressure of the gas and  $\rho_g$  the gas density. Using (6) and (8) we obtain (see also Cavaliere & Fusco-Femiano 1978):

$$\rho_g \propto \rho^{-\beta} \propto r^{-2\beta} \quad \text{with} \quad \beta = \frac{T}{T_g} = \frac{T}{T + T_{ad}} \quad (18)$$

Thus, for deep potential wells  $T \gg T_{ad}$  we have  $\beta \simeq 1$  and the gas follows the dark matter density profile while for cool clusters  $T \lesssim T_{ad}$  we get  $\beta \lesssim 1$  and the gas density profile is smoother than the dark matter distribution. This change of the shape of the gas density profile breaks the scaling (15) and it diminishes the luminosity of small clusters, through the variation of the factor  $n_e^2$  in (14), which leads to a steeper relation  $T - L_{bol}$ . Finally, we assume that the gas distribution extends to the virial radius  $R$  of the dark matter halo.

In the inner parts of the cluster, the density is large enough to lead to a small cooling time so that a cooling flow develops and some of the gas forms a cold component which does not emit in X-ray any longer. Thus, we define the cooling radius  $R_c$  as the point where the gas density reaches the threshold  $\rho_{gc}$  such that:

$$t_{cool} = t_H \quad \text{with} \quad t_{cool} = \frac{3\mu_1^2 m_p k T_g}{2\mu \rho_{gc} \Lambda_c(T_g)} \quad (19)$$

where  $\Lambda_c(T_g)$  is the cooling function (which is dominated by bremsstrahlung cooling for  $T > 1 \text{ keV}$ ) and  $t_H(z)$  is the Hubble time. At large radii  $r > R_c$  the density is lower than  $\rho_{gc}$  hence the local cooling time is larger than the Hubble time. Then, the gas distribution and the temperature had not had time to evolve much and the X-ray emissivity is proportional to  $\rho_g^2 \Lambda_b(T_g)$ , see (14). On the other hand, within the cooling radius  $R_c$  the gas had time to cool and form dense cold clouds. However, we consider

that some of the gas is still hot and emits in X-ray as cooling does not proceed in a uniform fashion (Nulsen 1986; Teyssier et al. 1997). The density of this hot component must be of order  $\rho_{gc}$  and we write the X-ray luminosity of the cluster as:

$$L_{bol} = \epsilon \left( \frac{\rho_{gc}}{\mu_e m_p} \right)^2 \Lambda_b(T_g) \frac{4\pi R_c^3}{3} \times \left\{ 1 + \frac{3}{4\beta - 3} \left[ 1 - \left( \frac{R_c}{R} \right)^{4\beta-3} \right] \right\} \quad (20)$$

where the factor 1 describes the contribution of the core, within  $R_c$ , and the second term comes from the halo. The factor  $\epsilon = 3$  is a parameter of order unity which we use to normalize our relation to observations for massive clusters ( $T_g > 1$  keV). We expect  $\epsilon \gtrsim 1$  which is indeed the case. It measures the density fluctuations of the gas distribution, since  $L_{bol} \propto \langle n_e^2 \rangle$  and at any radius  $\langle n_e^2 \rangle \gtrsim \langle n_e \rangle^2$  (however, using numerical simulations Mathiesen et al. 1999 obtain a smaller mean value  $\epsilon \simeq 1.4$ , but they do not include radiative cooling nor supernovae and simulations may miss some small scale power for the dark matter density distribution, see Valageas et al. 1999a and Valageas 1999). Our description is similar to the model developed by Cavaliere et al. (1997, 1998) to describe the relation between the gas and the dark matter density profile, which shows in the quantity  $\beta$ . However, while they define a core radius from the density distribution itself (because they use a dark matter profile which grows more slowly than  $r^{-2}$  at small  $r$ ) the core radius we use describes the cooling of the gas, independently of the profile of the underlying dark matter halo. We also considered density profiles for the dark matter of the form  $\rho \propto r^{-\gamma}$  with  $1.8 \leq \gamma \leq 2$ , where the gas density also shows a plateau for  $r \rightarrow 0$  before cooling. In all cases we obtain similar results, with a small dependence of  $T_{ad}$  on  $\gamma$  in order to match the same observations.

We show in Fig.6 the temperature-luminosity relation we obtain from (20). We see that our results agree with observations. In particular, the redshift evolution we get is very small, which is consistent with observations (Mushotzky & Scharf 1997).

## 6.2. Luminosity function

From the temperature-luminosity relation described in the previous section and the multiplicity function obtained in Sect.4 we can derive the cluster X-ray luminosity function, shown in Fig.7. Note that the results discussed in the following are largely independent of Sect.6 since any temperature-luminosity relation which agrees with observations would give similar results.

We see that our predictions agree reasonably well with the data for both cosmologies. However, as in Sect.4 and Sect.5 the redshift evolution is stronger for the critical

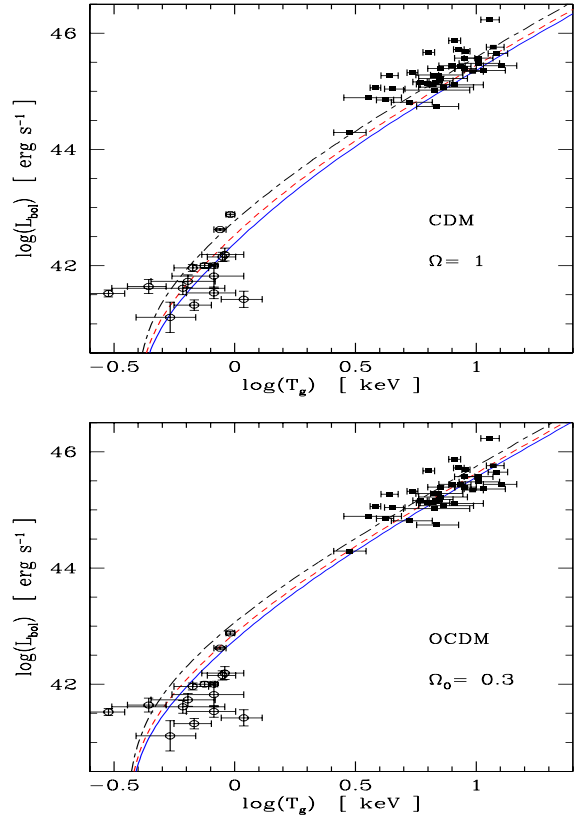


**Fig. 6.** *Upper panel:* the relation temperature - bolometric luminosity for clusters and groups, in the case  $\Omega = 1$ . The solid, dashed and dot-dashed lines correspond to  $z = 0$ ,  $z = 0.33$  and  $z = 1$  respectively. The data points are from Mushotzky & Scharf (1997) ( $0.14 < z < 0.55$ ) for clusters and from Ponman et al. (1996) ( $z < 0.05$ ) for groups. *Lower panel:* same curves for an open universe with  $\Omega_0 = 0.3$ .

universe, even though it remains quite modest. We also recover the fact that the scaling model predicts more massive and bright clusters but fewer small and faint objects than the PS approach.

We display in Fig.8 the integrated cluster surface density above an X-ray flux threshold  $S_X$  in the frequency band  $0.5 - 2$  keV:

$$\frac{dN}{d\Omega} (> S_X) = \int dz \frac{dV}{d\Omega dz} \int_{M'_i}^{\infty} \eta(M, z) \frac{dM}{M} \quad (21)$$

The cutoff  $M'_i(S_X, z)$  corresponds to the X-ray flux  $S_X$ . It is obtained through the temperature-luminosity relation (20) and the flux-luminosity relation:

$$S_X = \frac{L_X}{4\pi r_{lum}(z)^2} \quad (22)$$

with:

$$L_X = L_{bol} \left( e^{-h_P \nu_1(z)/kT} - e^{-h_P \nu_2(z)/kT} \right) \quad (23)$$

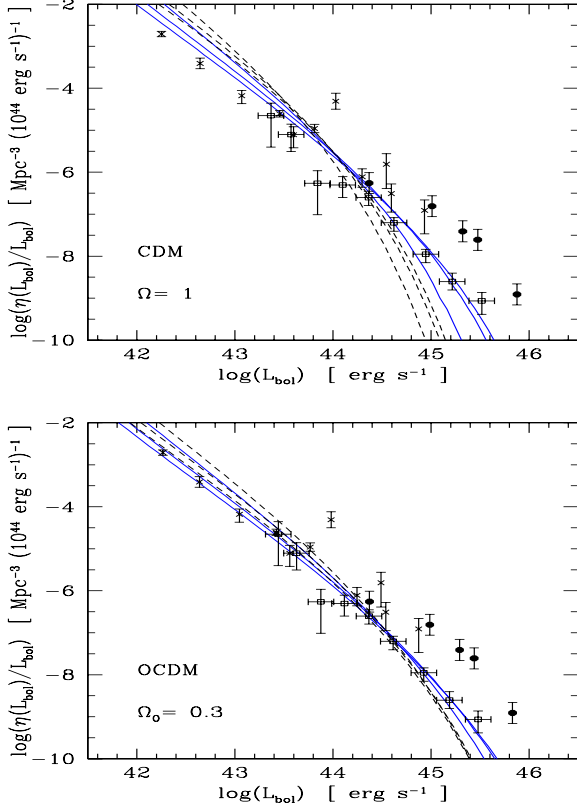


**Fig. 7.** *Upper panel:* the comoving cluster bolometric luminosity function for the case  $\Omega = 1$  at redshifts  $z = 0$ ,  $z = 0.33$  and  $z = 1$  (higher  $z$  corresponds to fewer bright objects). The solid line corresponds to the scaling formulation and the dashed line to the PS prescription. The data points at  $z = 0$  are from Henry & Arnaud (1991) (disks), Edge et al.(1990) (squares) and Burns (1996) (crosses). *Lower panel:* same curves for an open universe with  $\Omega_0 = 0.3$ .

Here  $h_P$  is Planck constant and  $\nu_i(z) = \nu_i(1+z)$  are the boundaries of the frequency band (0.5 – 2 keV). We neglected the variation of the Gaunt factor. The distance  $r_{lum}(z)$  is the luminosity distance to redshift  $z$ . Our results agree with observations although our normalization is a bit high for the critical density universe. In both panels, the dot-dashed curve corresponds to a no-evolution model where the comoving cluster luminosity function does not vary with  $z$  and remains equal to its value at  $z = 0$ , shown in Fig.7. Note that evolution effects are not very large. The scaling and PS approaches give very close results, although we can still recognize that the PS approximation predicts fewer massive objects but more small halos. Indeed, this difference is somewhat smeared out in Fig.8 because the X-ray sources seen with a given flux  $S_X$  consist of a large variety of objects located at different redshifts.

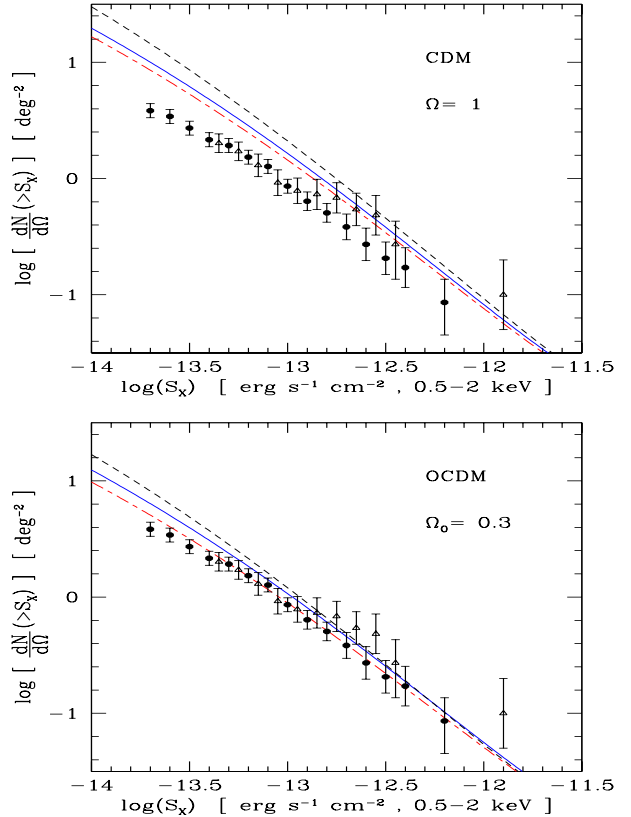


**Fig. 8.** *Upper panel:* the number of clusters per square degree brighter than an X-ray flux limit  $S_X$  for the case  $\Omega = 1$ . The solid line corresponds to the scaling formulation and the dashed line to the PS prescription. The dot-dashed curve is a no-evolution model. The data points are from Jones et al.(1998) (triangles) and Rosati et al.(1998) (disks). *Lower panel:* same curves for an open universe with  $\Omega_0 = 0.3$ .

## 7. Sunyaev-Zel'dovich effect

The variation of the CMB brightness at the frequency  $\nu$  along the line-of-sight due to the Sunyaev-Zel'dovich effect (Sunyaev & Zel'dovich 1972) can be written as (e.g. Barbosa et al.1996):

$$i_\nu = y j_\nu(x) \quad (24)$$

where  $j_\nu$  describes the spectral form of the distortion, independent of the cluster, and  $y$  is the Compton parameter given by an integration along the line-of-sight through the cluster:

$$y = \int n_e \sigma_T \frac{kT_g}{m_e c^2} dl \quad (25)$$

Here,  $T_g$  is the temperature of the electrons in the intracluster gas, given by (16),  $m_e$  the electron mass,  $n_e$  the electron number density and  $\sigma_T = 6.65 \cdot 10^{-25} \text{ cm}^2$  the Thompson cross section. Defining the dimensionless

frequency  $x = h_p \nu / kT_0 = \lambda_0 / \lambda$  where  $h_p$  is Planck's constant and  $\lambda_0 = 5.28$  mm for  $T_0 = 2.726$  K,  $T_0$  being the present temperature of the CMB, we can write:

$$j_\nu(x) = 2 \frac{(kT_0)^3}{(h_p c)^2} \frac{x^4 e^x}{(e^x - 1)^2} \left( \frac{x}{\tanh(x/2)} - 4 \right) \quad (26)$$

The flux  $S_\nu(x)$  of the cluster, in  $\text{mJy} = 10^{-26} \text{ erg s}^{-1} \text{cm}^{-2} \text{Hz}^{-1}$ , is simply the integral of  $j_\nu$  over the solid angle subtended by the cluster:

$$S_\nu(x) = j_\nu(x) r_d(z)^{-2} \int n_e \sigma_T \frac{kT_g}{m_e c^2} dV \quad (27)$$

where:

$$r_d(z) = \frac{2c}{H_0 \Omega_0^2 (1+z)^2} \left[ \Omega_0 z + (\Omega_0 - 2) \left( \sqrt{1 + \Omega_0 z} - 1 \right) \right]$$

is the angular distance of the cluster, located at redshift  $z$ . Hence, the total flux observed from an unresolved cluster depends only on the mass of gas at the temperature  $T_g$ , and not on the density profile. Moreover, we can see that  $y$  depends only on the physical properties of the cluster, and not on its redshift. Hence it is very sensitive to the cluster populations at high redshifts, which contribute in the same manner as close clusters, which means it is a useful tool to study the distant universe. Finally, in the long wavelength regime,  $x \rightarrow 0$ , the negative fluctuation of the CMB spectrum is simply given by:

$$\frac{\Delta T}{T} = -2y \quad (28)$$

The total mean Compton parameter  $\langle y \rangle$ , which only depends on the temperature distribution of the gas, can be obtained from (25) :

$$\langle y \rangle = \int c dt \int \sigma_T \frac{kT_g}{m_e c^2} \frac{d\bar{n}_e}{dT} dT \quad (29)$$

where  $\bar{n}_e$  is the mean electron number density. Whence:

$$\begin{aligned} \langle y \rangle &= \int_0^\infty dz \frac{dt}{dz} c \sigma_T (1+z)^3 \\ &\quad \times \int_{M_i}^\infty \frac{dM}{M} \eta(M) \frac{\Omega_b}{\Omega_0} \frac{M}{\mu_1 m_p} \frac{kT_g}{m_e c^2} \end{aligned} \quad (30)$$

The factor  $(1+z)^3$  transforms the comoving mass function  $\eta(M)$  we used so far into the mass function in proper coordinates. The cutoff at  $M_i(z)$  (defined by  $t_{cool} < t_H$ ) is due to the fact that in small halos the gas cools in less than one Hubble time  $t_H$ . The mass  $M_i(z)$  we get is typically of the order of  $10^{12} M_\odot$ .

An alternative way to get  $\langle y \rangle$  is to divide the line-of-sight into small length elements  $\Delta l_i$ , so that:

$$\langle y \rangle = \left\langle \sum_i \hat{y}_i \right\rangle \quad \text{and} \quad \langle y^2 \rangle = \left\langle \left( \sum_i \hat{y}_i \right)^2 \right\rangle \quad (31)$$

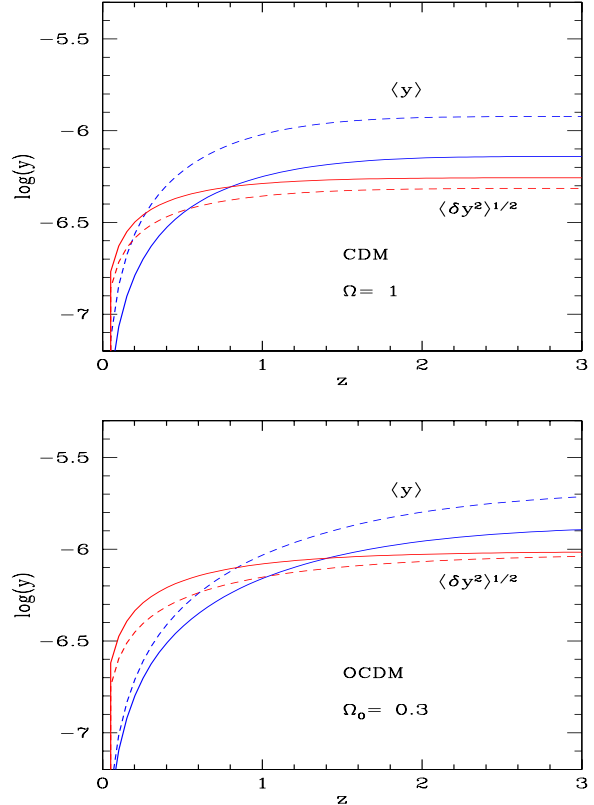


**Fig. 9.** *Upper panel:* the Compton parameter  $y$ , and its fluctuations  $\langle \delta y^2 \rangle^{1/2}$ , on a line-of-sight from  $z = 0$  up to the redshift  $z$ , for the case  $\Omega = 1$ . The solid lines correspond to the scaling formulation and the dashed lines to the PS prescription. In both cases the fluctuation  $\langle \delta y^2 \rangle^{1/2}$  is the curve which shows the steepest rise at  $z = 0$ . *Lower panel:* same curves for an open universe with  $\Omega_0 = 0.3$ .

where  $\hat{y}_i$  is the Compton distortion on the line element  $\Delta l_i$  in one random realization. In this way, we recover the previous formula (30) for  $\langle y \rangle$  and we get the fluctuations of  $y$ :

$$\langle \delta y^2 \rangle = \langle (y - \langle y \rangle)^2 \rangle \quad (32)$$

with:

$$\begin{aligned} \langle \delta y^2 \rangle &= \int_0^\infty dz \frac{dt}{dz} c \sigma_T (1+z)^3 \\ &\quad \times \left\{ \int_{M_i}^\infty \frac{dM}{M} \eta(M) \frac{\sigma_T}{\pi R^2} \left( \frac{\Omega_b}{\Omega_0} \frac{M}{\mu_1 m_p} \frac{kT_g}{m_e c^2} \right)^2 \right. \\ &\quad \left. + \sigma_T \Gamma(z) r_0(z) (1+z)^3 \left[ \int_{M_i}^\infty \frac{dM}{M} \eta(M) \frac{\Omega_b}{\Omega_0} \frac{M}{\mu_1 m_p} \frac{kT_g}{m_e c^2} \right]^2 \right\} \end{aligned} \quad (33)$$

The first term is due to the fluctuations of the number and luminosity of clusters in each line element, while the second term arises from the correlations among clusters, which we assume to be of the form  $\xi_{cc}(r, z) \sim (r/r_0(z))^{-\gamma}$ . The factor  $\Gamma(z)$  is of the order of:  $\Gamma(z) \sim (r_0/R)^{\gamma-1}$ , where

$R$  is the typical distance between close clusters. In the case  $\Omega = 1$ , we have  $\Gamma(z)r_0(z) \propto (1+z)^{-3}$  and the second term is small as compared to the first term. We note that the first term scales as  $\eta(M)$  while  $\langle y \rangle^2$  scales as  $\eta(M)^2$ . Thus, the fluctuations are important when the total number of clusters on the line of sight is small (see below Fig.12). Fig.9 shows the mean Compton parameter  $\langle y \rangle$  and its fluctuations  $\langle \delta y^2 \rangle^{1/2}$  on a line-of-sight from  $z = 0$  up to the redshift  $z$ . The Compton parameter  $\langle y \rangle$  is larger for the open universe because the cluster mass function declines more slowly at higher  $z$  and the line-element is slightly larger. Since the number of clusters on the line-of-sight is rather small the fluctuations of  $y$  are of the same magnitude as the mean  $\langle y \rangle$ . Of course  $\langle \delta y^2 \rangle^{1/2}$  is much larger than  $\langle y \rangle$  at  $z \simeq 0$  since the number of clusters tends to 0 in this limit. In particular, at  $z \simeq 0$  we have:

$$\langle y \rangle \propto [(1+z)^{3/2} - 1] \text{ and } \langle \delta y^2 \rangle^{1/2} \propto \langle y \rangle^{1/2} \quad (34)$$

Note that the COBE/FIRAS upper limit is  $\langle y \rangle < 1.5 \cdot 10^{-5}$  (Fixsen et al.1996). Thus, in both cosmologies the Sunyaev-Zel'dovich effect as measured by  $y$  is still one order of magnitude below the upper limit provided by present observations. Such a distortion, however, will be within the reach of the MAP and PLANK projects.

From the cluster mass function we can derive the flux density distribution of clusters  $\eta(S_\nu)dS_\nu/S_\nu$ . Hence, the number of SZ sources per unit solid angle on the sky with a total monochromatic flux greater than  $S_\nu$  (we assume that the objects are unresolved) is:

$$\frac{dN}{d\Omega}(>S_\nu) = \int dz \frac{dV}{d\Omega dz} \int_{M'_i}^\infty \eta(M, z) \frac{dM}{M} \quad (35)$$

The cutoff  $M'_i(S_\nu, z)$  corresponds to the threshold  $S_\nu$ . The SZ source counts at  $\lambda = 0.75$  mm are shown in Fig.10 as a function of  $S_\nu$  for both cosmologies. As for the Compton parameter  $y$  the open universe leads to slightly higher counts because of the slower decline of the cluster multiplicity function and of the larger volume element.

The redshift distribution of these source counts is displayed in Fig.11. Of course, as explained above, the open universe predicts a slower decline at large  $z$  of the source counts than for a critical universe.

## 8. Counts along the line-of-sight

In a fashion similar to the calculation of the Compton parameter  $y$  we can derive the mean number of clusters  $\mathcal{N}_{ls}(>M, < z)$  of mass larger than  $M$  which intersect a line-of-sight between  $z = 0$  and a given redshift  $z$ :

$$\mathcal{N}_{ls}(>M, < z) = \int_0^z c \frac{dt}{dz} (1+z)^3 dz \int_M^\infty \frac{dM}{M} \eta(M) \pi R^2$$

The result is displayed in Fig.12. As explained in Sect.4 and Sect.5 the scaling approach predicts more numerous

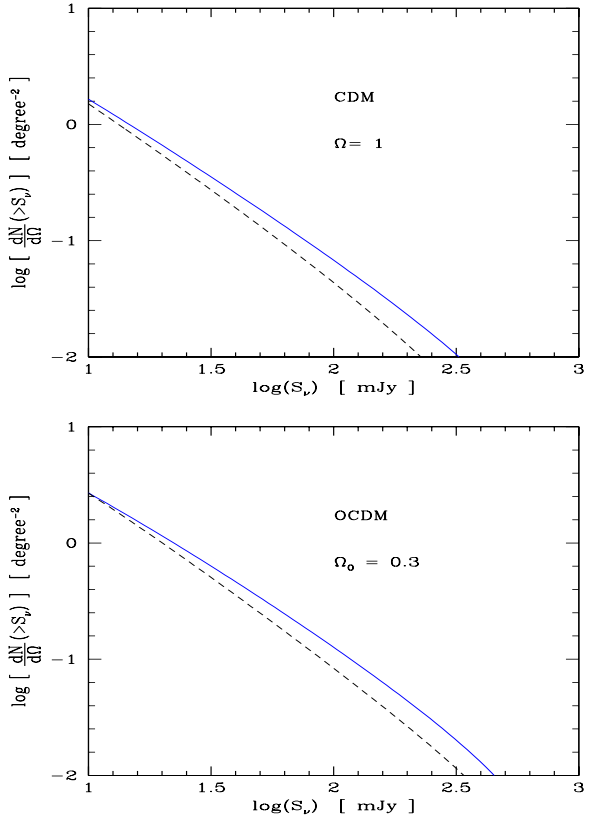


**Fig. 10.** *Upper panel:* the SZ source counts at  $\lambda = 0.75$  mm for the case  $\Omega = 1$ . The solid line corresponds to the scaling formulation and the dashed line to the PS prescription. *Lower panel:* same curves for an open universe with  $\Omega_0 = 0.3$ .

massive clusters and fewer small objects than the PS prescription. As described in Sect.7 the open universe gives higher counts for very massive halos. Note however that for the scaling prescription the difference between both cosmologies is quite small. Of course this would change with another choice for  $\sigma_8$ . We see that the mean number of clusters on a line-of-sight is quite small since we typically have  $\mathcal{N}_{ls} < 1$ . As discussed in Sect.7, this implies that the Compton parameter  $y$  obtained for different directions on the sky will show important fluctuations, see Fig.9.

## 9. Galaxies and quasars versus groups and clusters

### 9.1. Galaxy X-ray luminosity function

In order to form stars and become a galaxy the gas embedded within a dark matter halo must cool and fall into the gravitational potential well. During this process, the gas can radiate some energy in the X-ray band by bremsstrahlung, especially for the most massive galaxies with a large virial temperature  $T \sim 10^7$  K  $\sim 1$  keV. As a

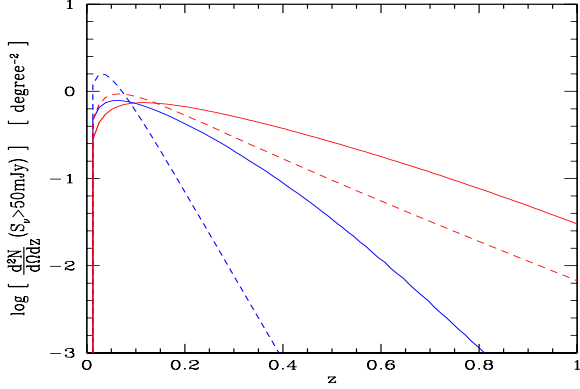


**Fig. 11.** The redshift distribution of SZ source counts for a critical and an open universe. The solid lines are the scaling formulation and the dashed lines the PS prescription. The low-density cosmology corresponds to the lowest decline at large  $z$  of the SZ counts.

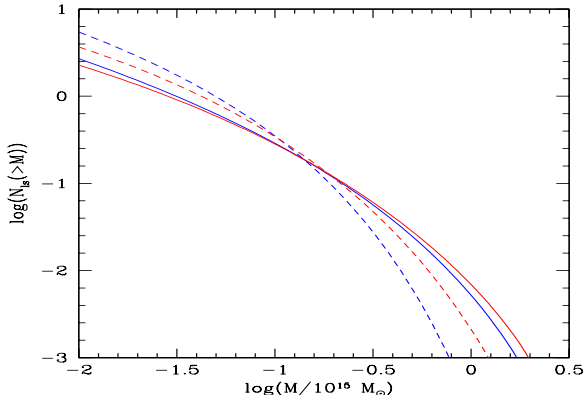


**Fig. 12.** The mean number of clusters  $N_{ls}(> M)$  of mass larger than  $M$  which intersect a line-of-sight between  $z = 0$  and  $z = 2$  (the contribution of higher redshifts is negligible). The solid lines correspond to the scaling prescription and the dashed lines to the PS approach. In both cases the number of very massive clusters is larger for the open universe.

consequence, some of the X-ray sources one could observe on the sky may be high-redshift newly-born galaxies. We can note that a theoretical and observational difficulty arises here when one wants to distinguish X-ray emitting galaxies from small groups which may only contain a handful of objects. Thus, the frontier we shall obtain between both classes of objects indicates a transitory range rather than a precise separation, especially since there is some scatter in the properties of real galaxies and groups.

To derive this galaxy X-ray luminosity function we use the galaxy formation model described in details in Valageas & Schaeffer (1999). This previous study is consistent with the present work (all parameters have the same values) and it was checked against observations for various

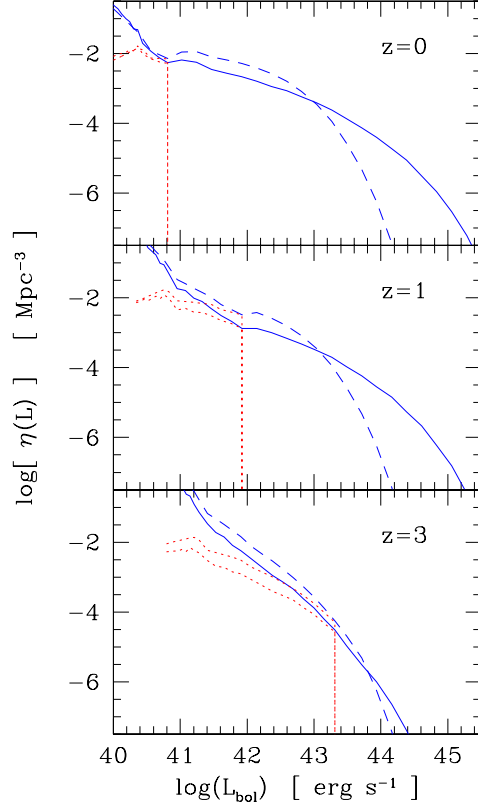


**Fig. 13.** The comoving galaxy bolometric luminosity function for the case  $\Omega = 1$ . The solid line corresponds to the scaling formulation and the dashed line to the PS prescription where we do not take into account the effect of cooling (cutoff at  $T_f$  and prefactor  $t_{cool}/t_H$ ). The dotted lines show the actual luminosity functions for both prescriptions with the proper effects of cooling.

galaxy properties. We briefly recall here the characteristics of this model we need for our purposes. We define galaxies by the requirement that two constraints be satisfied by the underlying dark matter halo: 1) a *virialization condition*  $\Delta > \Delta_c$  and 2) a *cooling constraint*  $t_{cool} < t_H(z_{form})$  which states that the gas must have been able to cool within a few Hubble times at formation. We assume that the Hubble time at formation is given by the dynamical time, i.e. that the density of these dark matter halos does not evolve much after collapse. Note that just-collapsed halos ( $\Delta = \Delta_c$ ) verify  $t_{dyn} \sim t_H$  by definition. Thus, the dark matter radius of the halos we identify with galaxies is given by:

$$t_{cool} < t_{dyn} \quad \text{and} \quad \rho > (1 + \Delta_c) \bar{\rho} \quad (36)$$

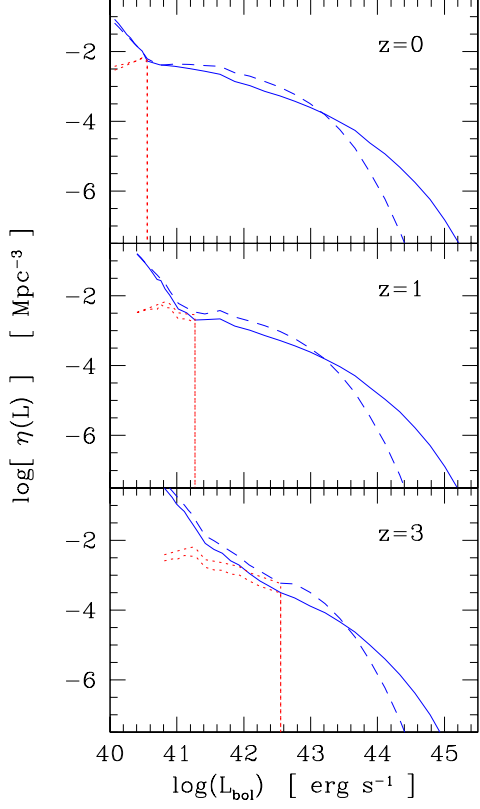


**Fig. 14.** The comoving galaxy bolometric luminosity function for the case  $\Omega_0 = 0.3$ . Same curves as in Fig.13.

In other words, the radius  $R(T, z)$  of galaxies of virial temperature  $T$  at redshift  $z$  is:

$$R(T, z) = \text{Min} (R_{cool}, R_{vir}) \quad (37)$$

where  $R_{cool}$  is a “cooling radius” defined by  $t_{cool} = t_{dyn}$  while  $R_{vir}$  is the virial radius. At low redshift, for small virial temperature  $T$  cooling is very efficient so that the virialization condition is the most stringent one in (36). Hence  $R = R_{vir}$  and these galactic halos are defined by the usual density contrast threshold  $\Delta_c(z)$ . On the other hand, for large temperature cooling is inefficient so that galactic halos are defined by  $R = R_{cool}$ . This means that their mean density contrast is larger than  $\Delta_c$  and that these objects formed at a larger redshift than the one considered (as opposed to just-collapsed objects defined by  $\Delta = \Delta_c$ ). At large  $T$ , where bremsstrahlung is the main cooling process, the cooling radius tends to a constant  $R_{cool} \sim 100$  kpc.

Thus, at any  $z$  there is a characteristic virial temperature  $T_f(z)$  which marks the transition between these two regimes. It increases with  $z$  and at  $z = 0$  we have  $T_f \sim 10^6$  K. In this approach, large objects defined by  $\Delta = \Delta_c$  with a virial temperature  $T > T_f(z)$  are made of several

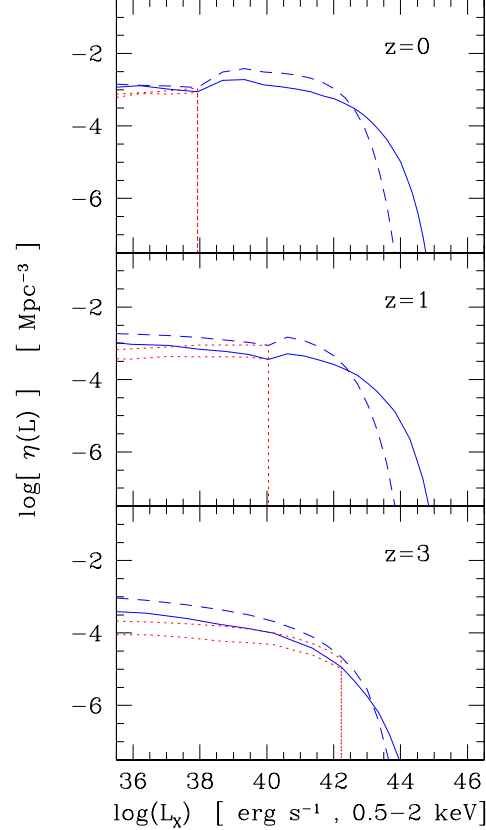


**Fig. 15.** The comoving galaxy X-ray luminosity function in the frequency band  $0.5 - 2$  keV for the case  $\Omega = 1$ . The solid line corresponds to the scaling formulation and the dashed line to the PS prescription where we do not take into account the effect of cooling (cutoff at  $T_f$  and prefactor  $t_{cool}/t_H$ ). The dotted lines show the actual luminosity functions for both prescriptions with the proper effects of cooling.

galaxies and correspond to groups or clusters. They can be subdivided into several subunits which verify the constraints (36). Of course, halos with a virial temperature which is only slightly higher than  $T_f(z)$  merely consist of one galaxy with some gas falling from its surroundings which have not cooled yet. However, we shall identify just-collapsed halos above  $T_f(z)$  as groups or clusters, which should provide a reasonable estimate of the transition, while we shall call just-collapsed halos below  $T_f(z)$  as galaxies. Thus, the bright and massive galaxies above  $T_f$  which formed earlier make no contribution to the galactic X-ray flux seen at the considered epoch. Indeed, in this approach since they formed at a higher redshift  $z_{form}$  with  $t_{cool} \sim t_H(z_{form})$  their gas has already cooled and fallen into the galactic potential well so that there is no more X-ray emission. However, they contribute to the galactic

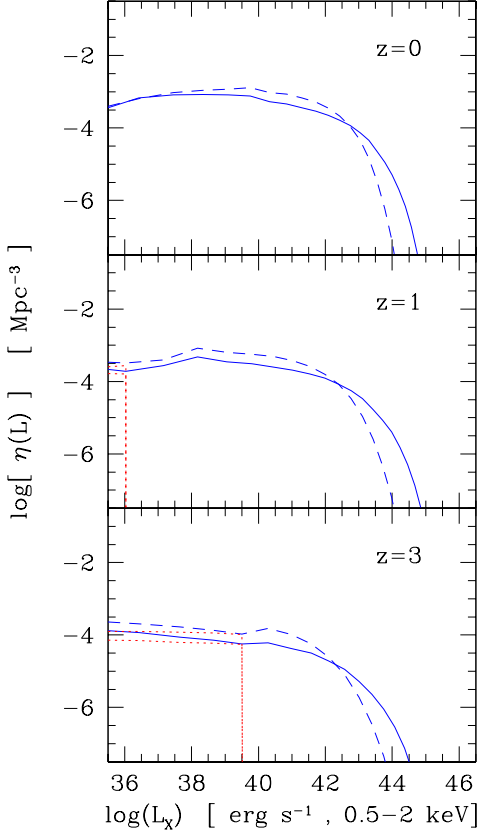


**Fig. 16.** The comoving galaxy X-ray luminosity function in the frequency band 0.5 – 2 keV for the case  $\Omega_0 = 0.3$ . Same curves as in Fig.15.

X-ray luminosity at redshift  $z_{form}$ . Moreover, they are embedded within groups or clusters which radiate in the X-ray band, and which we have considered in the previous sections. In particular, the mass functions of groups and clusters we used above were set to 0 for  $T < T_f(z)$  (this also corresponds to the cutoff  $M_i(z)$  which appeared in (30) to obtain  $\langle y \rangle$ ). However, this has no effect on the quantities we studied so far because we considered high virial temperatures  $T > 0.5$  keV at low redshifts  $z < 1$ .

We write the galaxy luminosity (due to cooling of the gas) as:

$$L_{bol} = \frac{E}{t_{cool}} = \frac{3}{2} \frac{M_g k T}{\mu m_p t_{cool}} \quad (38)$$

Then, using the multiplicity functions described in Sect.2 we can derive the galaxy X-ray luminosity function. However, note that for galaxies above  $T_f$  which are no longer defined by the constant density contrast threshold  $\Delta_c(z)$  we must modify our prescription. In fact the scaling formulation remains almost unchanged: the density contrast which enters the definition (2) of the variable  $x$  is merely

changed from  $\Delta_c(z)$  to  $\Delta(M, z)$  which is the actual density contrast of these galactic halos. Since the PS approach can be translated into the scaling prescription it can also be modified in a similar fashion. This is described in details in Valageas & Schaeffer (1999) (see also VS). However, we do not really need the galaxy mass function in this range since, as explained above, we do not identify these galaxies as individual X-ray emitting sources. We shall only plot their multiplicity functions in the figures for reference. In addition to the cutoff  $T_f(z)$ , cooling introduces a second effect for the galaxy X-ray luminosity function. Indeed, galaxies with  $T < T_f(z)$  verify by definition  $t_{cool} < t_H(z)$ . Although they are defined as “just-collapsed” objects ( $\Delta = \Delta_c$ ) in practice they have undergone a major merging event recently ( $\delta z/(1+z) \ll 1$ ) but all of them are not necessarily in the midst of such a process. Since the time which elapsed since the last merging is measured by  $t_H$  we write for the galaxy X-ray luminosity function:

$$\eta(L) \frac{dL}{L} = \frac{t_{cool}}{t_H} \eta(M) \frac{dM}{M} \quad (39)$$

which takes into account the fact that some of the small galaxies (where  $t_{cool} \ll t_H$ ) have already cooled since their last merging event.

We show in Fig.13 and Fig.14 the galaxy X-ray luminosity functions we obtain in this way for both cosmologies. The solid lines (resp. dashed lines) correspond to the scaling formulation (resp. the PS prescription) without the cutoff at  $T_f$  and the prefactor  $t_{cool}/t_H$  which appears in (39). As explained above the cutoff  $T_f(z)$  increases with  $z$  which leads to a higher luminosity cutoff  $L_f(z)$  at larger  $z$ . Below  $T_f$  the prefactor  $t_{cool}/t_H$  diminishes the contribution of small and faint galaxies since an increasingly large fraction of these objects is cold. At the virial temperature  $T_f(z)$  we have  $t_{cool} = t_H$  by definition so that the curves coincide at the cutoff. Note that, as was the case for the cluster multiplicity functions, the scaling approach predicts more massive objects and fewer intermediate halos than the “PS prescription” (above  $T_f$  it is not the usual PS mass function but an extended formulation). As usual, the redshift evolution is smaller for the open universe. The galaxy multiplicity function evolves more slowly (for the same reason as for the cluster multiplicity function) and the cutoff  $T_f(z)$  increases less quickly with  $z$ . This is mainly due to the fact that the density  $(1 + \Delta_c)(z)\bar{\rho}(z)$  grows more slowly than  $(1 + z)^3$  at low  $z$  because of the variation of  $\Delta_c(z)$ , which leads to a smaller change for  $T_f(z)$ .

We display in Fig.15 and Fig.16 the galaxy X-ray luminosity function in the frequency band 0.5 – 2 keV. We recover the same behaviour as for the X-ray bolometric luminosity function shown in Fig.13 and Fig.14. However, the contribution of small galaxies (which have a low virial temperature  $T$ ) is strongly suppressed because of the factors  $\exp(-h_P \nu / kT)$ . For the open universe the luminosity

function evolves more slowly except for the cutoff  $L_{Xf}(z)$  which increases faster with  $z$  than for the case  $\Omega = 1$ . This is due to the fact that the temperature attached to these galaxies (in particular  $T_f$ ) is somewhat smaller for the low-density universe which implies that the factors  $\exp(-h_P \nu / kT)$  are more sensitive on  $T_f$  and evolve faster with  $z$ . Note that the X-ray luminosity  $L_{Xf}(z)$  is indeed lower for the open universe.

### 9.2. Quasar X-ray luminosity function

In addition to galaxies, groups and clusters, quasars are important sources of X-ray radiation. In fact, as we shall see in the next section their contribution to the X-ray flux is much larger than the galactic emission because of their harder radiation spectrum (which is roughly similar to a power-law as opposed to the black-body spectrum of stars). Thus, it is of interest to estimate the quasar source counts since they dominate at fluxes smaller than those corresponding to clusters. Moreover, it allows us to obtain a complete description of X-ray objects within the framework of a unified model. Indeed, we use the quasar multiplicity function which was built in Valageas & Silk (1999a) to study the reheating and reionization history of the universe. It is fully consistent with the cluster and galaxy mass functions we obtained in the previous sections. In particular, the quasar luminosity function is derived from the galaxy multiplicity function since in our model QSOs correspond to the central parts of some galaxies where some accreting gas shines at the Eddington limit. We refer the reader to Valageas & Silk (1999a) for a detailed description of our model. From the quasar multiplicity function we obtain the X-ray source counts which are identified as QSOs as in (21). We assume the quasar spectrum is locally a power-law  $L_\nu \propto \nu^{-1.5}$  around  $\nu_1 = 1$  keV, normalized by  $(L_1/L_{bol}) = 0.028$  with  $L_1 = \nu_1 L_\nu(\nu_1)$ .

We present in Fig.17 and Fig.18 the comoving quasar luminosity function we obtain for both cosmologies  $\Omega = 1$  and  $\Omega_0 = 0.3, \Omega_\Lambda = 0$ . The frequency band  $0.5 - 2$  keV corresponds to the observed spectrum (i.e. the light was emitted between  $0.5(1+z)$  and  $2(1+z)$  keV). We see that we obtain a reasonable agreement with observations from Miyaji et al.(1998), both at low redshift  $z \sim 0.3$  and high redshift  $z \sim 3.5$ . As explained in Valageas & Silk (1999a) the high luminosity cutoff of our quasar luminosity function comes from the fact that in our model very massive and bright galaxies have already consumed most of their gas which leads to an upper bound for the quasar luminosity at low  $z$ . Note moreover that our predictions also agree with the observed quasar luminosity function in the B band, as seen in Valageas & Silk (1999a).

### 9.3. Galaxy and quasar versus group and cluster counts

From the X-ray luminosity functions obtained in the previous sections we can derive the surface density on the sky of

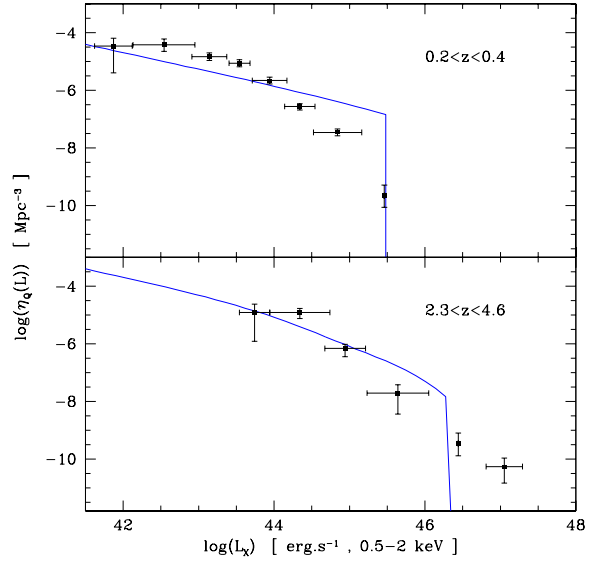


**Fig. 17.** The comoving quasar X-ray luminosity function in the frequency band  $0.5 - 2$  keV for the case  $\Omega = 1$ . The data points are observations from Miyaji et al.(1998).

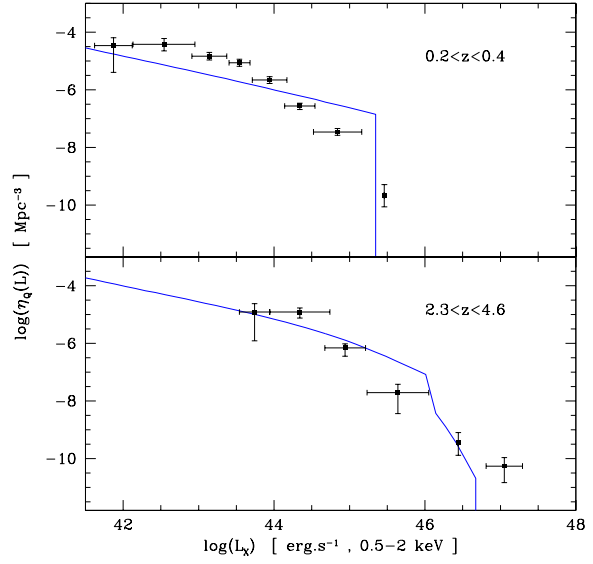


**Fig. 18.** The comoving quasar X-ray luminosity function in the frequency band  $0.5 - 2$  keV for the case  $\Omega_0 = 0.3$ .

sources brighter than an X-ray flux limit  $S_X$ , taking into account the contribution from galaxies as well as from QSOs, groups and clusters. We show our results for the scaling model in Fig.19. We see that the contribution from individual galaxies, although restricted to very low fluxes  $S_X < 10^{-17} \text{ erg s}^{-1} \text{ cm}^{-2}$ , dominates at  $S_X \sim 10^{-18}$  (for the critical universe). This is due to their smaller mass and temperature, as well as to their higher redshift of formation, but to their larger number, as compared to groups.

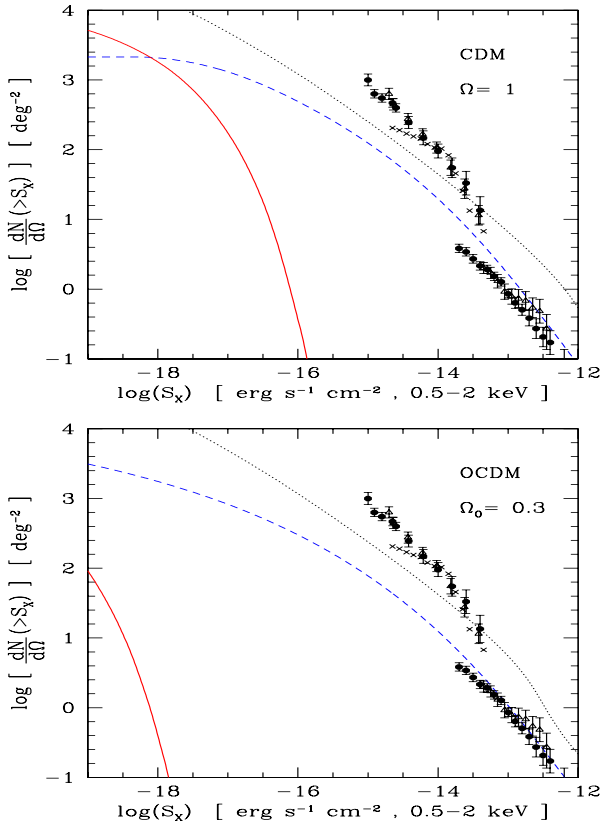


**Fig. 19.** *Upper panel:* the number of sources per square degree brighter than an X-ray flux limit  $S_X$  for the case  $\Omega = 1$ . The solid line corresponds to galaxies and the dashed line to groups and clusters. The dotted line shows the quasar number counts. We only display the scaling model. The data points for quasars are from Hasinger et al.(1998) (disks for the 1112 ksec PSPC and triangles for the 207 ksec HRI) and McHardy et al.(1998) (crosses). The data points for clusters are as in Fig.8. *Lower panel:* same curves for an open universe with  $\Omega_0 = 0.3$ .

The galaxy contribution is much smaller for the open universe because of the lower cutoff  $L_{Xf}$ , as seen in Fig.15 and Fig.16. *The observation of these X-ray emitting galaxies would provide a direct signature of galaxy formation and of the associated cooling process.* Bright galaxies start to appear already at  $S_X \sim 10^{-16}$ , typically one per square degree, and are within the AXAF sensitivity limits<sup>1</sup>. In our model (see Valageas & Schaeffer 1999), such bright galaxies typically correspond to a virial temperature of  $10^7 K$ , a Baryon mass of  $2.310^{11} M_\odot$ . It is just forming at  $z = 3$ , with an x-ray luminosity of  $1.510^{43} \text{ erg/s}$  over a time of  $1.410^9$  years. As we noticed above, however, due to theoretical and observational ambiguities the most relevant curve is probably the sum of both contributions from galaxies and groups. Then, we see that the predictions

<sup>1</sup> We are indebted to R. Mushotzky for a discussion of this point.

obtained for both cosmologies are similar. On the other hand, because of their harder radiation spectrum quasars provide an important contribution to the X-ray source counts, a relative contribution that is increasing at fluxes somewhat below the typical values of groups and clusters. We note that although we recover the right abundance of AGN source counts at high luminosities  $S_X \sim 10^{-14} \text{ erg s}^{-1} \text{ cm}^{-2}$  we somewhat underestimate the number of low luminosity objects  $S_X \sim 10^{-15} \text{ erg s}^{-1} \text{ cm}^{-2}$ . This may suggest that a more detailed model of QSOs is needed in order to match exactly the observations. On the other hand, we note that McHardy et al.(1998) find that at low fluxes a new population of sources appears which consists of narrow emission lines galaxies which could partly correspond to starburst galaxies, which we did not specifically include in our model.

## 10. Summary and Conclusion

We have examined the predictions of the *scaling model* for the number of X-ray emitting objects as a function of redshift. This approach gives the multiplicity of non-linear structures directly from the non-linear density field, and should be considered as an improvement over the PS approximation. This model gives more precise counts and can also be used for any density contrast, much larger than the usual value of 200 as well as much smaller. It also solves the hierarchy (cloud-in-cloud) problem and allows to describe structures embedded within other virialized condensations. This method thus allows to simultaneously describe galaxies (and quasars) as well as galaxy clusters. We also built a simple model for the luminosity of clusters which agrees with the observed temperature - X-ray luminosity relation.

For the temperature and the X-ray luminosity distribution, the counts obtained in this way typically differ by a factor of two from the PS approximation, but the differences may reach an order of magnitude for extreme cases (very large or very small objects). With an initial CDM spectrum that is normalized in the same way as in the numerical simulations that reproduce the same data, the scaling model reproduces the currently available observations, while the PS approximation does not (the latter would, provided the normalization of the power spectrum is modified). The evolution with redshift is different too, for reasons that are well understood. The counts for  $T > 5 \text{ kev}$ , or for  $M > 5 \cdot 10^{14} M_\odot$ , for instance, peak at  $z = 0.4$  rather than  $z = 0.2$  for  $\Omega = 1$ , with a much larger normalization.

This allows a more accurate estimation of the Sunyaev-Zel'dovich distortion parameter  $y$  along a given line of sight (summing over the contribution of clusters). For the same CDM initial conditions as above, we get  $\langle y \rangle = 2 \cdot 10^{-6}$  that induces fluctuations  $\langle \delta y^2 \rangle^{1/2} = 10^{-6}$  in the CMB for  $\Omega_0 = 0.3$ , and values a factor of two smaller in a critical

universe, the bulk of the contribution arising from clusters at  $z < 1$ .

The source counts above a given X-ray flux limit show that, while quasars provide a dominant contribution, for increasing sensitivity one gets access to smaller groups which cool faster than the present Hubble time but were quite luminous in the past, as well as, in the extreme case, to galaxies forming at redshifts of 2 or 3 during their quite rapid cooling period. These objects, that were luminous in the past and start appearing in the past for deep enough surveys, are undoubtedly a new challenge. They are accessible with the current sensitivity of AXAF.

## References

Arnaud M., Evrard A.E., 1999, MNRAS 305, 631

Balian R., Schaeffer R., 1989, A&A 220, 1

Barbosa D., Bartlett J.G., Blanchard A., Oukbir J., 1996, A&A 314, 13

Bernardeau F., Schaeffer R., 1991, A&A, 220, 23

Bernardeau F., Schaeffer R., 1992, A&A, 225, 1

Bernardeau F., Schaeffer R., 1999, A&A, in press

Blanchard A., Valls-Gabaud D., Mamon G., 1992, A&A 264, 365

Bond J.R., Cole S., Efstathiou G., Kaiser N., 1991, ApJ 379, 440

Bouchet F.R., Schaeffer R., Davis M., 1991, ApJ 383, 19

Burns et al., 1996, ApJ 467, L49

Cavaliere A., Fusco-Femiano R., 1978, A&A 70, 677

Cavaliere A., Menci N., Tozzi P., 1997, ApJL 484, L21

Cavaliere A., Menci N., Tozzi P., 1998, astro-ph 9810498

Cole S., Lacey C., 1996, MNRAS 281, 716

Colombi S., Bernardeau F., Bouchet F.R., Hernquist L., 1997, MNRAS 287, 241

Davis M., Efstathiou G.P., Frenk C.S., White S.D.M., 1985, ApJ 292, 371

Edge A.C., Stewart G.C., Fabian A.C., Arnaud K.A., 1990, MNRAS 245, 559

Eke V.R., Cole S., Frenk C.S., 1996, MNRAS 282, 263

Eke V.R., Navarro J.F., Frenk C.S., 1998, ApJ 503, 569

Elvis M., Wilkes B.J., McDowell J.C., Green R.F., Bechtold J., Willner S.P., Oey M.S., Polomski E., Cutri R., 1994, ApJS 95, 1

Evrard A.E., 1990, ApJ 363, 349

Evrard A.E., Henry J.P., 1991, ApJ 383, 95

Evrard A.E., Metzler C.A., Navarro J.F., 1996, ApJ 469, 494

Fixsen D.J., Cheng E.S., Gales J.M., Mather J.C., Shafer R.A., Wright E.L., 1996, ApJ 473, 576

Governato F., Babul A., Quinn T., Tozzi P., Baugh C.M., Katz N., Lake G., 1999, submitted to MNRAS, astro-ph 9810189

Hasinger G., Burg R., Giacconi R., Schmidt M., Trumper J., Zamorani G., 1998, A&A 329, 482

Henry J.P., Arnaud K.A., 1991, ApJ 372, 410

Henry J.P., 1997, ApJ 489, L1

Jones L.R., Scharf C., Ebeling H., Perlman E., Wegner G., Malkan M., Horner D., ApJ 1998, 495, 100

Kaiser N., 1986, MNRAS 222, 323

Mc Hardy I.M., Jones L.R., Merrifield M.R., et al., 1998, MNRAS 295, 641

Mathiesen B., Evrard A.E., Mohr J.J., 1999, to appear in ApJL, astro-ph 9904429

Miyaji T., Hasinger G., Schmidt M., 1998, Proceedings of "Highlights in X-ray Astronomy", astro-ph 9809398

Munshi D., Bernardeau F., Melott A. L., Schaeffer R., 1999, MNRAS 303, 433

Mushotzky R.F., Scharf C.A., 1997, ApJ 482, L13

Navarro J.F., Frenk C.S., White S.D.M., 1995, MNRAS 275, 720

Navarro J.F., Frenk C.S., White S.D.M., 1996, ApJ 462, 563

Nulsen P.E.J., 1986, MNRAS 221, 377

Oukbir J., Bartlett J.G., Blanchard A., 1997, A&A 317, 10

Peacock J.A., Heavens A.F., 1990, MNRAS 243, 133

Ponman T.J., Bourner P.D., Ebeling H., Bohringer H., 1996, MNRAS 283, 690

Ponman T.J., Cannon D.B., Navarro J.F., 1999, Nature 397, 135

Press W.H., Schechter P., 1974, ApJ 187, 425

Rosati P., Della Ceca R., Norman C., Giacconi R., 1998 ApJ 492, L21

Sunyaev R.A., Zel'dovich Y.B., 1972, Comm. Astrophys. Space Phys., 4, 173

Teyssier R., Chieze J.-P., Alimi J.-M., 1997, Proc. "A new vision of an old cluster", eds. F.Durret et al., France, astro-ph 9710010

Valageas P., Schaeffer R., 1997, A&A 328, 435 (VS)

Valageas P., Schaeffer R., 1999, A&A 345, 329

Valageas P., 1999, A&A, 347, 757

Valageas P., Silk J., 1999a, A&A 347, 1

Valageas P., Silk J., 1999b, accepted by A&A, astro-ph 9907068

Valageas P., Lacey C., Schaeffer R., 1999a, accepted by MNRAS, astro-ph 9902320

Valageas P., Schaeffer R., Silk J., 1999b, A&A 345, 691

Wu K.K.S., Fabian A.C., Nulsen P.E.J., 1998, submitted to MNRAS, astro-ph 9810008